













Three-dimensional chromatin mapping of sensory neurons reveals that promoter–enhancer looping is required for axonal regeneration

Ilaria Palmisano^{a,b,1,2} , Tong Liu^{c,1}, Wei Gao^a , Luming Zhou^a, Matthias Merkschlager^d , Franziska Mueller^a , Jessica Chadwick^a , Rebecca Toscano Rivalta^a, Guiping Kong^a, James W. D. King^d, Ediem Al-jibury^d, Yuyang Yan^a , Alessandro Carlino^b , Bryce Collison^b , Eleonora De Vitis^b , Sree Gongala^a, Francesco De Virgiliis^a, Zheng Wang^{c,2,3}, and Simone Di Giovanni^{a,3} 

Affiliations are included on p. 11.

Edited by Roman Giger, University of Michigan Medical School, Ann Arbor, MI; received February 9, 2024; accepted August 10, 2024 by Editorial Board Member Yishi Jin

The in vivo three-dimensional genomic architecture of adult mature neurons at homeostasis and after medically relevant perturbations such as axonal injury remains elusive. Here, we address this knowledge gap by mapping the three-dimensional chromatin architecture and gene expression program at homeostasis and after sciatic nerve injury in wild-type and cohesin-deficient mouse sensory dorsal root ganglia neurons via combinatorial Hi-C, promoter-capture Hi-C, CUT&Tag for H3K27ac and RNA-seq. We find that genes involved in axonal regeneration form long-range, complex chromatin loops, and that cohesin is required for the full induction of the regenerative transcriptional program. Importantly, loss of cohesin results in disruption of chromatin architecture and severely impaired nerve regeneration. Complex enhancer–promoter loops are also enriched in the human fetal cortical plate, where the axonal growth potential is highest, and are lost in mature adult neurons. Together, these data provide an original three-dimensional chromatin map of adult sensory neurons in vivo and demonstrate a role for cohesin-dependent long-range promoter interactions in nerve regeneration.

nerve regeneration | three-dimensional chromatin architecture | cohesin | regeneration program | promoter loops

Hi-C studies have revealed that the genome is folded into self-interacting regions known as topologically associating domains (TADs) or contact domains, which regulate gene transcription by spatially restricting and facilitating enhancer–promoter (E–P) interactions (1–4). The three-dimensional (3D) chromatin organization allows enhancers to loop over long genomic distances to engage with target gene promoters, affecting gene transcription by providing binding sites for transcription factors (TFs) and chromatin remodelers, and by recruiting RNA polymerase II machinery and RNA polymerase II regulators (5, 6). Such 3D organization arises from the coordinated activity of cohesin and CCCTC-binding factor (CTCF) (7–10). According to the loop extrusion model, the ring-like cohesin complex translocates on the DNA in an ATP-dependent way progressively extruding bidirectional chromatin loops until it is halted by CTCF bound in a convergent orientation (11, 12).

Despite the critical role of 3D genome looping in gene regulation, the in vivo map of the chromatin architecture in mature adult neurons at homeostasis and after injury remains elusive. Similarly, whether chromatin organization and E–P interactions are modified by loss of neuronal homeostasis and whether these interactions play a role in axonal regeneration after injury remain undetermined. The axonal regenerative capacity in the peripheral nervous system is underpinned by the coordinated changes in the expression of hundreds of genes involved in multiple interconnected biological processes (13–15). Studies in the dorsal root ganglia (DRG), which contain sensory neurons, have shown that histone acetylation, DNA methylation, and hydroxymethylation contribute to the regenerative transcriptional program after nerve injury by affecting chromatin accessibility at promoters and enhancers of regenerative genes (15–24). However, they did not show an absolute requirement of these epigenetic mechanisms for nerve regeneration, and they did not account for the role of 3D chromatin folding in the regulation of gene expression after injury. Furthermore, when systemic studies were performed, they were conducted from bulk DRG tissue and did not discriminate between neurons versus stromal and glial cells (15, 25, 26).

Significance

The mechanisms underpinning axon regeneration after injury remain only partially understood. This work shows that three-dimensional chromatin architecture is required for the activation of the axonal regeneration program and for nerve regeneration. Nerve regeneration is supported by cohesin, which generates long and complex promoter–enhancer loops at regenerative genes. This work shows that, in addition to previously recognized epigenetic mechanisms at the level of the linear genome, the three-dimensional chromatin architecture, such as promoter–enhancer interactions, should be considered as an added layer of transcriptional regulation in the response to nerve injury. These findings have broad implications for neuronal biology and future repair strategies.

The authors declare no competing interest.

This article is a PNAS Direct Submission. R.G. is a guest editor invited by the Editorial Board.

Copyright © 2024 the Author(s). Published by PNAS. This article is distributed under [Creative Commons Attribution-NonCommercial-NoDerivatives License 4.0 \(CC BY-NC-ND\)](https://creativecommons.org/licenses/by-nc-nd/4.0/).

¹I.P. and T.L. contributed equally to this work.

²To whom correspondence may be addressed. Email: ilaria.palmisano@osumc.edu or zheng.wang@miami.edu.

³Z.W. and S.D.G. contributed equally to this work.

This article contains supporting information online at <https://www.pnas.org/lookup/suppl/doi:10.1073/pnas.2402518121/-/DCSupplemental>.

Published September 10, 2024.

Here, we provide a chromatin architecture map of in vivo mature sensory neurons and determine the role of neuronal 3D chromatin organization and promoter–enhancer looping in gene expression regulation at homeostasis and after a nerve injury. To this end, we performed Hi-C, promoter-capture Hi-C (PCHi-C), RNA-seq, and CUT&Tag (Cleavage Under Targets and Tagmentation) for H3K27ac in purified DRG neuronal nuclei following sciatic nerve crush (SNC) from wild-type (WT) and *Rad21* (cohesin structural subunit) conditional knock-out (KO) mice. We show that 3D chromatin organization and the formation of promoter interactions at regenerative genes are required for nerve regeneration. Genes induced in response to injury form longer and more frequent chromatin loops, which are enriched in the human developing cortex where neuronal growth is highest. Importantly, cohesin is required for full activation of regenerative genes and loss of cohesin prevents axonal regeneration in vivo. These data provide an in vivo neuronal 3D chromatin and gene expression map at homeostasis, revealing a central role for 3D genome architecture in regulating regenerative gene expression, and identifying cohesin as a critical regulator of nerve regeneration.

Results

Neuronal Cohesin Depletion Abrogates Nerve Regeneration.

Given the role of cohesin and CTCF in 3D genome organization and chromatin looping, we took advantage of published transcriptomic datasets from purified DRG neurons at homeostasis and following nerve injury (27) as well as ChIP-seq datasets of CTCF and Structural Maintenance of Chromosomes 1 (SMC1, cohesin subunit) from neuronal tissue (28–30) to examine the binding of CTCF and cohesin to the promoters of genes at homeostasis and after axonal injury. A high proportion of neuronal promoters displayed binding sites for cohesin at both homeostatic and injury conditions (Dataset S1). Specifically, 47.5% of the injury-responsive promoters showed binding sites for cohesin, while only 27.3% showed binding sites for CTCF (SI Appendix, Fig. S1A). Interestingly, genes with cohesin binding sites were enriched for biological processes associated with regenerative ability including nervous system development, neuronal differentiation, axon projection and guidance, microtubule organization, axon transport, and synapse organization (13, 31, 32) (SI Appendix, Fig. S1B and Dataset S2). However, genes with CTCF binding sites were less enriched for such biological processes (SI Appendix, Fig. S1B and Dataset S2). By screening published transcriptomic datasets from purified cortical and retinal ganglion neurons in regenerative conditions (33, 34), we found that neuronal promoters displayed binding sites for cohesin and CTCF, and that a higher proportion of genes showed preferential binding to cohesin over CTCF, as in DRG neurons (SI Appendix, Fig. S1A and Dataset S1). Although genes with cohesin binding sites showed a higher enrichment for biological processes associated with regenerative ability, genes with CTCF binding sites were also associated with multiple regenerative pathways (SI Appendix, Fig. S1B and Dataset S2).

Altogether, these data suggest that 3D genome architecture mechanisms might regulate gene expression that is required for nerve regeneration in response to injury and that cohesin might have a preferential role with respect to CTCF.

To test this hypothesis, we assessed nerve regeneration in cohesin-depleted versus WT DRG neurons. To this end, we conditionally deleted the cohesin subunit *Rad21*, which is required for the integrity of the cohesin complex (35), as well as cohesin-mediated chromatin looping and domain organization (7–10). We injected

AAV-Cre-GFP or AAV-GFP in the sciatic nerves of *Sccl flox/flox* mice (35) 4 wk before a SNC. Nerve regeneration was assessed by measuring the intensity of Stathmin-like 2 (STMN2 or SCG10) immunolabeling, as a marker of regenerating axons (36). Neuron-specific loss of RAD21 (SI Appendix, Fig. S2 A–C) resulted in a strong impairment of nerve regeneration at 7 d after nerve crush (Fig. 1 A–C). Furthermore, 14 d after nerve crush, we injected cholera toxin subunit B (CTB) in the *tibialis anterioris* and *gastrocnemius* muscles, to specifically trace DRG neurons that regenerated their axons across the injury site into the muscle. The number of CTB-positive DRG neurons was significantly reduced in RAD21-depleted mice (Fig. 1 D and E). Consistently, we found a severe reduction in epidermal reinnervation 18 d post injury, as assessed by counting the number of Ubiquitin C-terminal hydrolase L1 (UCHL1 or PGP9.5) positive fibers in the hind paw interdigital skin (Fig. 1 F–H). This defect in nerve regeneration was not due to neuronal death, as established by staining for active caspase-3 and by counting the number of DRG neurons per surface unit (SI Appendix, Fig. S2 D–F); instead, it was associated with loss of regenerative associated genes (RAGs) activation as shown by ATF3 and c-Jun expression studies (SI Appendix, Fig. S3).

Together, these data show that cohesin is required for nerve regeneration and suggest that cohesin-dependent chromatin 3D architecture mechanisms might underpin the regenerative program after injury.

Cohesin Is Required for the Activation of Neuronal Regenerative Genes and Pathways Following Injury.

Next, we investigated whether cohesin is required for the establishment of the gene expression program that follows nerve injury and supports regeneration. To this end, we performed RNA-seq from WT or *Rad21* conditionally deleted DRG neuronal nuclei in naïve conditions as well as 3 d after SNC versus sham control. We took advantage of the isolation of nuclei tagged in specific cell types (INTACT) mouse (37) and generated INTACT-AdvillinCre mice (Methods) that express a superfolded GFP-Myc tagged version of SUN1 (nuclear membrane protein) in Advillin positive cells following tamoxifen injection (SI Appendix, Fig. S4A). Since Advillin is expressed in all sensory neurons (38), this allows purification of the DRG sensory neuronal nuclei at high yield and purity (SI Appendix, Fig. S4 B–D). We then crossed INTACT-AdvillinCre mice with *Sccl flox/flox* mice to induce uniform depletion of RAD21 in DRG neurons (SI Appendix, Fig. S5). Sixteen days after tamoxifen injection, RNA-seq was performed. Spearman correlation and principal component analysis (PCA) of the RNA-seq data showed high reproducibility between replicates (SI Appendix, Fig. S6 and Dataset S3). RNA-seq confirmed a 70% loss of *Rad21* expression in DRG neurons (Dataset S4). RAD21 depletion induced downregulation of 711 and upregulation of 283 genes in naïve conditions (FDR < 0.05) (SI Appendix, Fig. S7A and Dataset S4). Following injury, the number of differentially expressed genes increased, with 1,093 down-regulated and 694 up-regulated genes (FDR < 0.05) (SI Appendix, Fig. S7B and Dataset S4).

To investigate the biological significance of the genes affected by the lack of cohesin, we performed a gene ontology (GO) analysis of the differentially expressed genes in *Rad21* KO versus WT neurons in different conditions. In naïve condition, *Rad21* deletion induced the downregulation of genes involved in neuronal-specific functions, such as ion transport and neurotransmitter signaling (Fig. 2A, first column, and Dataset S5). In agreement with previous findings (15, 27, 31, 32, 39, 40), in WT neurons nerve injury triggered regenerative pathways as shown by the expression of genes involved in transcription, immune regulation, nervous system developmental

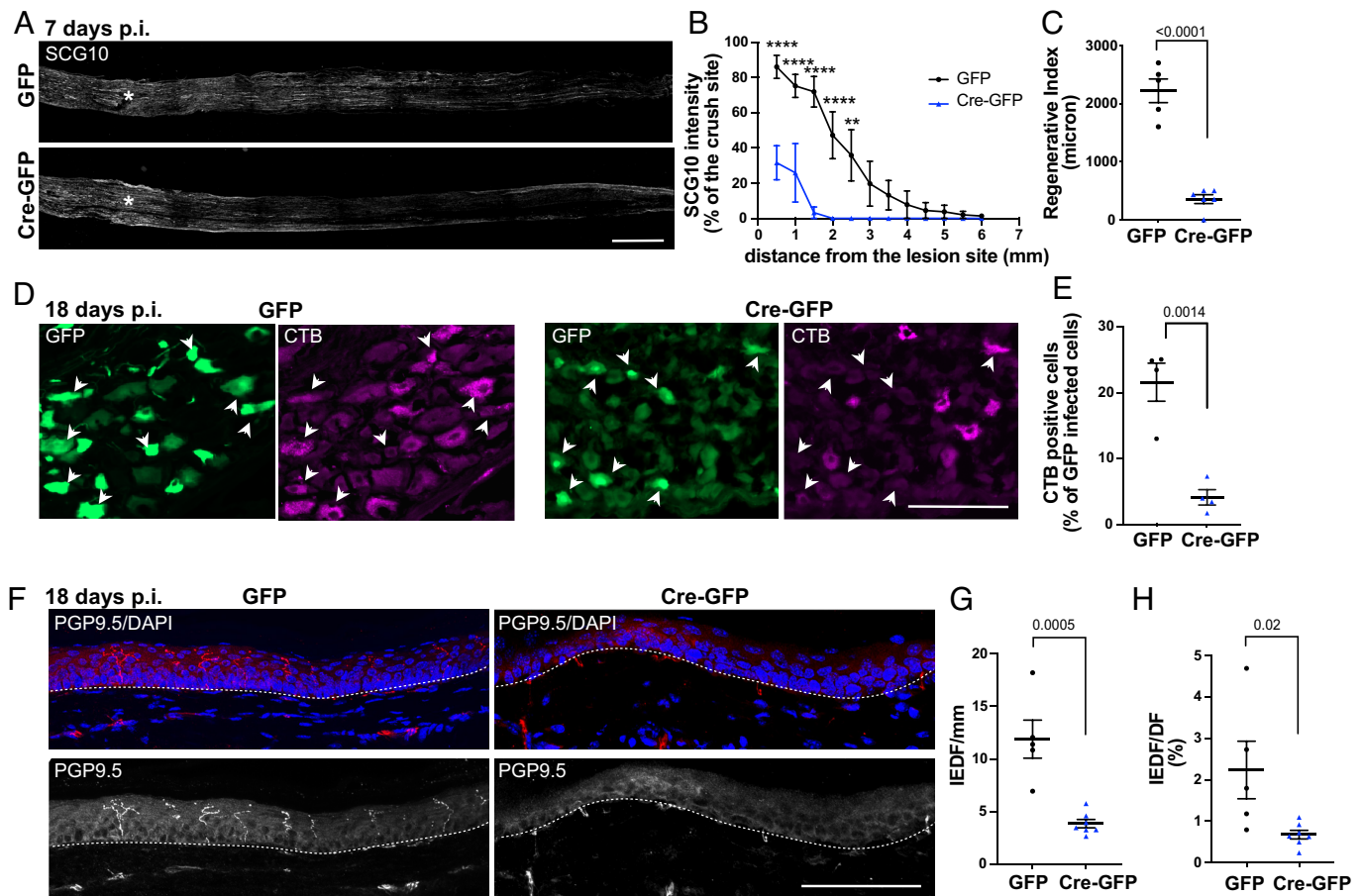


Fig. 1. Loss of cohesin impairs nerve regeneration. (A and B) Representative micrographs and quantification of SCG10 intensity at the indicated distances from the lesion site in sciatic nerves from AAV-GFP or AAV-Cre-GFP injected *Scc1flox/flox* mice at 7 d following SNC. The asterisk marks the lesion site. (Scale bar, 1 mm.) (mean \pm SEM of $n = 5$ nerves from four AAV-GFP mice and $n = 6$ nerves from four AAV-Cre-GFP mice; **** $P < 0.05$, **** $P < 0.0001$, two-way ANOVA, Sidak's multiple comparisons test). (C) Bar charts of the regeneration index in AAV-GFP or AAV-Cre-GFP injected *Scc1flox/flox* mice at 7 d after SNC (mean \pm SEM of $n = 5$ nerves from four AAV-GFP mice and $n = 6$ nerves from four AAV-Cre-GFP mice; two-sided unpaired Student's *t* test). (D) Micrographs showing GFP (green) and CTB (magenta) signal in DRG 4 d after injection of CTB in the tibialis anterioris and gastrocnemius muscle 14 d after SNC. Arrowheads mark GFP-positive neurons. (Scale bar, 100 μ m.) (E) Bar graphs of the CTB positive neurons as percentage of GFP expressing neurons (mean \pm SEM of $n = 4$ mice; two-sided unpaired Student's *t* test). (F) Representative micrographs of PGP9.5 immunostaining with DAPI counterstaining in the interdigital hind-paw skin from AAV-GFP or AAV-Cre-GFP injected *Scc1flox/flox* mice 18 d after SNC. The dashed lines indicate the boundary between the epidermis and dermis. (Scale bar, 100 μ m.) (G and H) Quantification of the number of intraepidermal fibers (IEF) per millimeter of interdigital skin and the percentage of IEDF versus dermal fibers (DF) (mean \pm SEM of $n = 5$ skins from four AAV-GFP mice; $n = 7$ skins from four AAV-Cre-GFP mice; two-sided unpaired Student's *t* test).

processes, signal transduction, cytoskeleton remodeling, circadian rhythms, axonogenesis, angiogenesis, cell adhesion, reactive oxygen species signaling, and downregulation of genes involved in ion transport and synaptic transmission (Fig. 2A, second column, *SI Appendix*, Fig. S7C, and *Dataset S5*). However, in RAD21-depleted neurons, most of the genes belonging to regenerative pathways either failed to be activated at all by injury, or were induced at lower levels, or were down-regulated compared to WT neurons (Fig. 2A, third and fourth columns and *Dataset S5*). Genes that were down-regulated after injury in WT neurons were also down-regulated in *Rad21* KO neurons. Genes that remained inducible or were up-regulated in the absence of cohesin were enriched for categories involved in the inflammatory response (Fig. 2A, third and fourth columns, and *Dataset S5*). This suggests that cohesin is specifically required for the activation of the regenerative transcriptional program in response to injury.

To directly explore this hypothesis, we analyzed constitutive homeostatic genes (genes that were not differentially regulated after SNC versus Sham in WT neurons, $n = 23,008$) and genes that were activated by injury (up-regulated after SNC versus Sham) in WT neurons ($n = 1,230$), separately. Only between 3.4 and 5.5% of the constitutive genes were differentially expressed

in *Rad21* KO versus WT neurons in naïve and injury conditions, respectively (Fig. 2B, *Top*). In striking contrast, 21.2% of the injury-activated genes were down-regulated in *Rad21* KO versus WT neurons following injury, but not in naïve conditions (Fig. 2B, *Bottom*). Only 6.0% of the injury-activated genes were up-regulated in *Rad21* KO neurons following injury.

We then assessed the expression pattern of the 1,230 injury-activated genes, in *Rad21* KO and WT neurons. We found that 651 genes were still fully inducible and up-regulated in *Rad21* KO neurons after SNC versus Sham to WT levels or higher (Fig. 2C, *SI Appendix*, Fig. S7D, cohesin-independent, and *Dataset S6*). These cohesin-independent genes were enriched for immune-related functions (Fig. 2D, *Left*). We found 579 genes that were either down-regulated in injured cohesin-depleted neurons with respect to WT or that were not inducible after injury. Among these 579 cohesin-dependent genes, 106 were partially inducible but exhibited a lower baseline expression and a decreased response to injury (Fig. 2C, *SI Appendix*, Fig. S7D, cohesin-dependent, inducible, and *Dataset S6*) and 473 genes failed to respond to injury (Fig. 2C, *SI Appendix*, Fig. S7D, cohesin-dependent, not inducible, and *Dataset S6*). Cohesin-dependent genes were mainly enriched for actin cytoskeleton remodeling, axon guidance, neuron development,

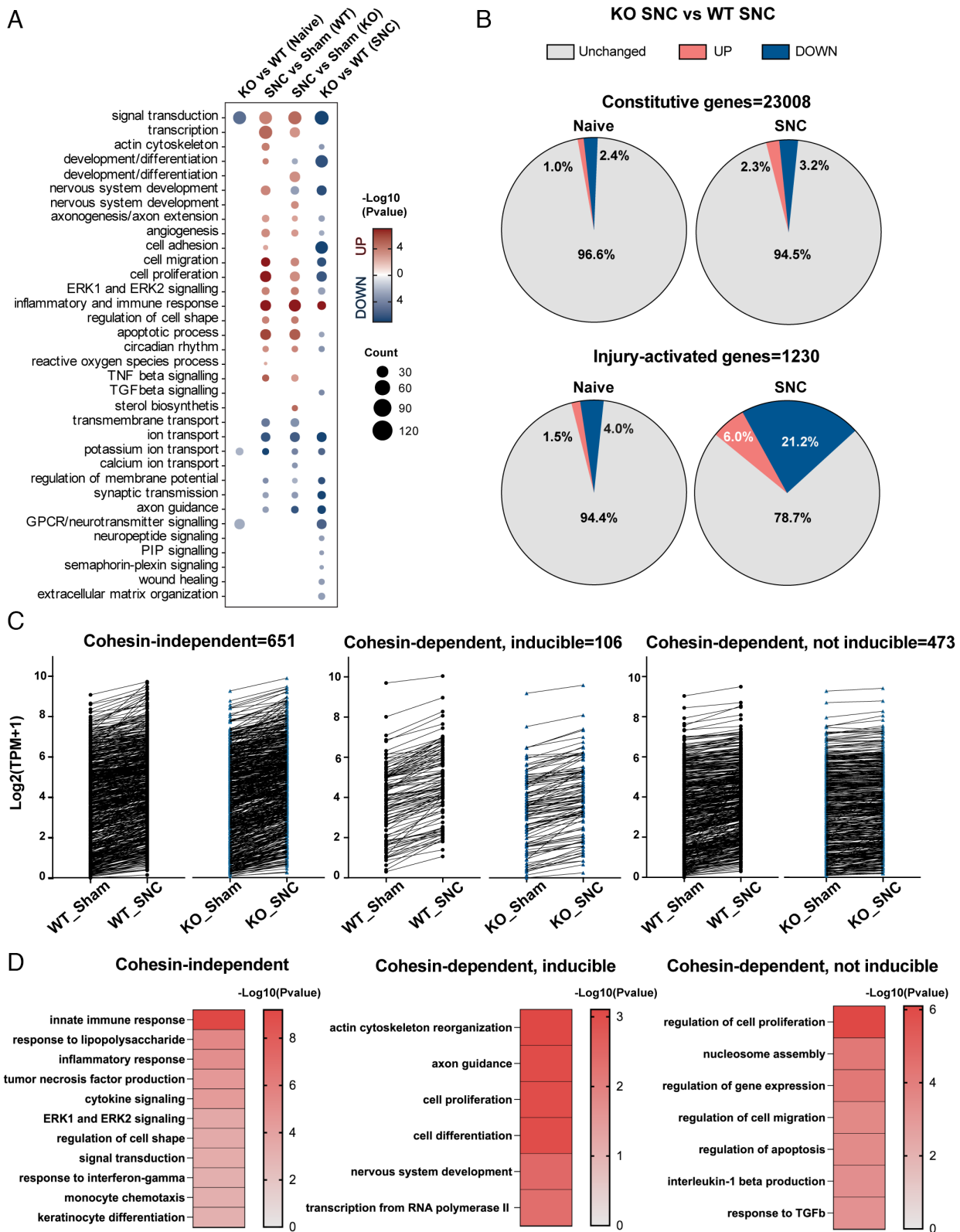


Fig. 2. Cohesin-dependent and independent genes. (A) Dot plot of the semantically clustered GO biological process categories of the up-regulated (red) and down-regulated (blue) genes in the indicated conditions. Color code reflects the P -value (modified Fisher's exact $P \leq 0.005$) and the size of the dot the gene count in each category (gene count > 6). (B) Pie charts of the expression of constitutive (Top) and injury-activated (Bottom) genes in *Rad21* KO neurons in naïve and injured conditions ($n = 3$ independent samples; $FDR < 0.05$). (C) Line plots of the expression in the indicated conditions of the cohesin-independent and dependent (inducible and noninducible) genes (TPM = transcripts per million). (D) Heatmaps of the semantically clustered GO biological process categories of the cohesin-dependent and independent genes. Color code reflects the P -value (modified Fisher's exact $P \leq 0.001$).

signaling, RNA polymerase II-dependent transcription, nucleosome assembly, and immune-modulation pathways (Fig. 2 D, Middle and Right). Accordingly, we found that the lack of cohesin impaired the

injury-driven activation of RNA polymerase II, with only modest effects on the steady-state levels of the active enzyme (SI Appendix, Fig. S8).

Altogether, these data indicate that cohesin is required for the transcriptional response to injury that is related to the regenerative potential by controlling the expression of genes involved in regenerative pathways.

Cohesin-Dependent 3D Chromatin Architecture Is Required for the Activation of Neuronal Regenerative Genes Following Injury. In cortical neurons, cohesin is required for the activation of activity-dependent genes that form long-range chromatin loops (41). To explore whether cohesin facilitates long-range chromatin loops between the promoters of injury-responsive genes and their regulatory elements, we leveraged recently published deep Hi-C studies in mouse cortical neurons (42). We found that injury-activated genes were involved in longer loops compared to constitutive homeostatic genes (*SI Appendix, Fig. S9* and *Dataset S7*). Importantly, cohesin-dependent genes were associated with more frequent and longer loops compared to cohesin-independent genes (*SI Appendix, Fig. S9 B–D* and *Dataset S7*). Several RAGs were found among the injury-activated genes and involved in longer loops (*SI Appendix, Fig. S9D* and *Dataset S7*). These data suggest a key role for cohesin-dependent 3D genome organization in the coordination of the transcriptional response to injury in DRG neurons.

To gain additional insights into the role of the 3D genomic architecture of DRG neurons in the transcriptional regulation at homeostasis versus nerve injury, we next performed Hi-C from WT and RAD21-depleted DRG neurons 3 d following SNC versus sham by using the same inducible-INTACT-AdvillinCre mouse model used for RNA-seq (Fig. 3A). Stratum-adjusted correlation coefficients (SCC) scores of the Hi-C data showed high reproducibility between replicates (*SI Appendix, Fig. S10* and *Dataset S3*). After aligning and filtering an average of 712 million Hi-C sequenced read pairs, we obtained an average of 210 million long-range (>20 Kb) intrachromosomal contacts (MAPQ > 0; for details, see *Dataset S3*). A/B compartments and chromatin 3D domains were called on replicate-pooled, balanced Hi-C contact matrices (*SI Appendix, Supplementary Methods*). We identified 7,662, 7,683, and 7,753 domains in WT neurons in naïve, sham, and injury conditions, respectively (see *Dataset S8* for the domains' definitions in all the conditions).

Hi-C revealed that *Rad21* KO in DRG neurons resulted in mild effects on global genome A/B compartmentalization (*SI Appendix, Fig. S11*), whereas it strongly disrupted the organization of 3D chromatin domains in both naïve and injury conditions (Fig. 3 B–F). Cohesin-depleted neurons showed a loss of insulation at 3D domain boundaries (Fig. 3 B and D) and led to the loss of 5,873 and 4,598 domains in naïve and injury conditions, respectively (see *Dataset S9* for the lost, conserved, and gained domains). We also observed a genome-wide reduction in contact frequency as a function of the genomic distance in cohesin-depleted versus WT neurons (Fig. 3C). The distance between the “within domains” and “between domains” curves was strongly decreased indicating a loss of the chromatin contacts in cohesin-depleted neurons (Fig. 3C). We then normalized and balanced the Hi-C contact frequencies (*SI Appendix, Supplementary Methods*) coupled with RNA-seq to identify changes in chromatin interactions within domains and their correlation with gene expression between WT and *Rad21* KO neurons. We identified 6,624 and 5,359 domains with a lower interaction frequency (FDR < 0.05) in naïve and injury conditions, respectively, (Fig. 3E and *Dataset S10*). Differentially expressed, mainly down-regulated, genes were more strongly associated with domains showing a decreased frequency of interaction (Fig. 3F and *Dataset S10*).

Down-regulated genes residing in genomic domains that were lost or showed a reduction in strength in *Rad21* KO neurons were enriched for regenerative pathways, such as axon extension and guidance, nervous system development, neuronal differentiation, circadian rhythm, angiogenesis, actin cytoskeleton remodeling (15, 31, 32, 39, 40) (Fig. 4A). The previously identified 579 cohesin-dependent genes (Fig. 2C and *Dataset S6*), including several RAGs, were preferentially found within domains that were lost or showed a reduction in strength in *Rad21* KO neurons (Fig. 4 B–D).

Altogether, these data indicate that cohesin activates the transcriptional response to injury that is related to the regenerative potential by controlling the 3D chromatin architecture of genes involved in regenerative pathways (Fig. 4E).

Cohesin-Dependent Neuronal Genes Form Complex Long-Range Chromatin Loops After Injury. To explore whether cohesin facilitates chromatin loops between the promoters of injury-responsive genes and their regulatory elements, we performed PCHi-C from WT and RAD21-depleted DRG neurons 3 d following SNC versus homeostasis (sham) (Fig. 3A). An average of 312 million read pairs were generated for each sample of PCHi-C, with a total of 3.7 billion read pairs generated (*Dataset S3*). Significant loops were called using CHiCAGO pipeline (43) (*SI Appendix, Supplementary Methods*). The majority of promoters in both WT and *Rad21* KO neurons were involved in more than one interaction, however, *Rad21* KO neurons displayed fewer interactions compared to WT, globally (*SI Appendix, Fig. S12, Left*). Indeed, we identified 36,158 and 43,438 loops in WT neurons at homeostasis (sham) and SNC conditions, respectively, whereas, in RAD21-depleted neurons, a lower number of loops were identified (27,069 and 31,210 in sham and after SNC, respectively) (*Dataset S11*). In both uninjured and injured conditions, active genes were characterized by a higher number of chromatin interactions with respect to genes that were not expressed or expressed at a very low level (inactive) (Fig. 5A). This pattern was not observed in *Rad21* KO neurons, suggesting loss of regulatory interactions (Fig. 5A). Furthermore, in WT neurons, promoters engaged in larger loops following injury with respect to homeostasis (sham) conditions; instead, in *Rad21* KO neurons, promoter loops were globally shorter (Fig. 5B). Next, we inspected the features of promoter loops of the injury-activated genes in WT neurons. In agreement with our previous analysis of cortical neuron loops (*SI Appendix, Fig. S9*), we found that they were involved in longer loops after injury in comparison with the sham condition, however, this was not observed in *Rad21* KO neurons (Fig. 5C).

We then compared the 3D chromatin features of the cohesin-dependent versus cohesin-independent genes (*Dataset S12*). While both cohesin-dependent and independent genes engaged in longer loops after injury with respect to sham control in WT neurons (Fig. 5D, 1.11 and 1.31 loop length ratio between SNC versus sham in cohesin-independent and dependent genes, respectively), the average loop length following injury was higher in cohesin-dependent genes with respect to cohesin-independent genes (Fig. 5D, 1.28 loop length ratio between cohesin-dependent versus cohesin-independent genes). In particular, genes that were noninducible in response to injury in *Rad21* KO neurons displayed the largest change in loop length in response to nerve injury in WT neurons with respect to the ones that were still partially inducible in *Rad21* KO neurons (Fig. 5E, 1.13 and 1.40 loop length ratio between SNC versus sham in cohesin inducible and noninducible genes, respectively). Furthermore, cohesin-dependent genes showed a higher number of loops that form in response to nerve injury with respect to cohesin-independent genes (Fig. 5F).

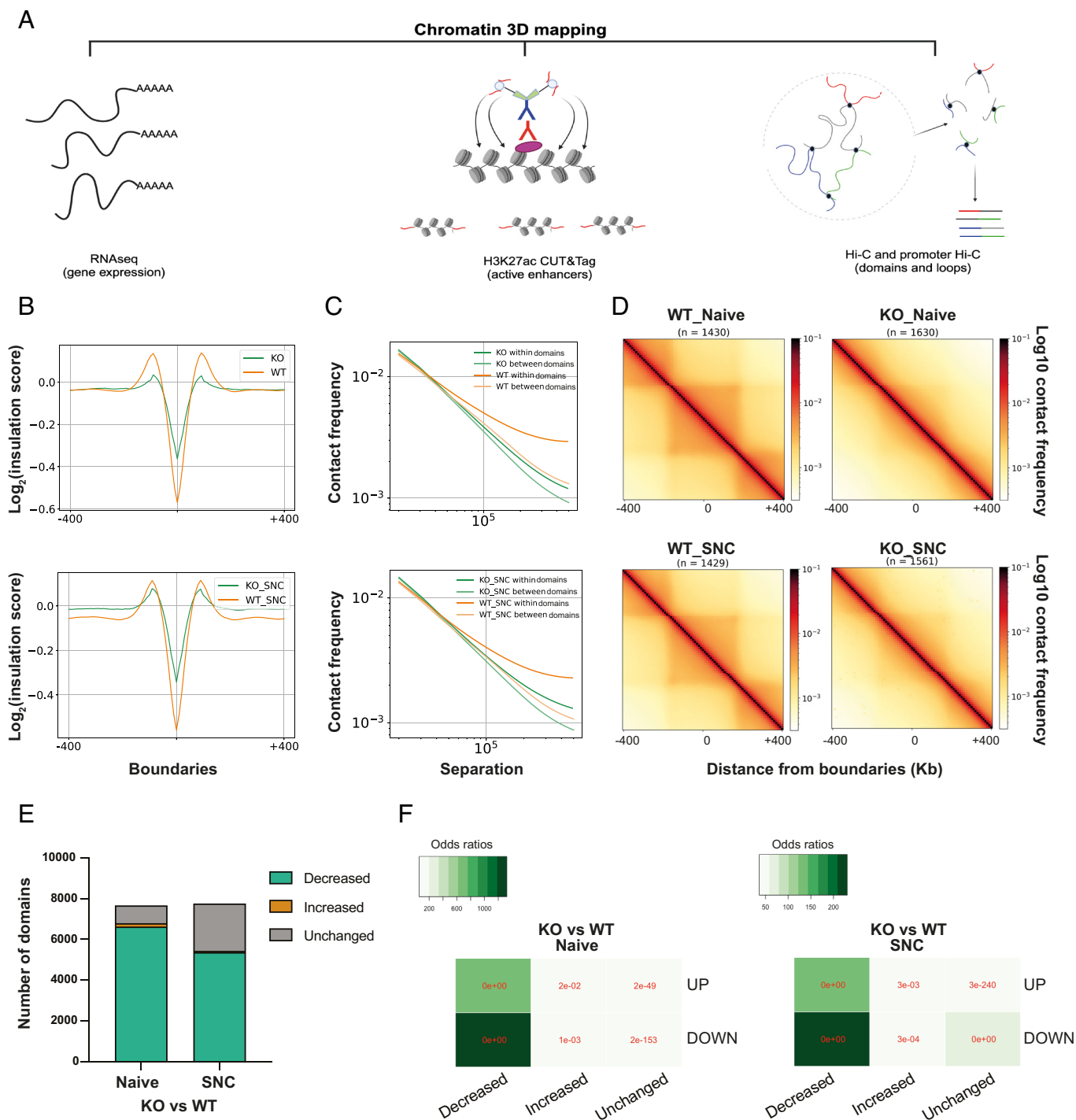


Fig. 3. Loss of cohesin leads to a decrease in chromatin interactions. (A) Schematic of the chromatin mapping in DRG neurons. (B) Genome-wide plot of the averaged insulation scores around strong boundaries (the size of flanks around each strong boundary is 400 Kb) in the indicated conditions. (C) P(s) curve (contact probability versus genomic distance) within and between genomic domains of length 300 to 500 Kb for the indicated conditions. (D) Average Hi-C contact matrices at 10-Kb resolution of the indicated number of 3D chromatin domains of length 300 to 400 Kb in the indicated conditions. (E) Bar charts of the number of 3D chromatin domains showing an average increased, decreased, and unchanged frequency of contacts ($n = 3$ independent samples; FDR < 0.05). (F) Odds ratios analysis of the association between up- and down-regulated genes and differentially expressed genes present in increased, decreased, or unchanged domains; the numbers in red represent the P -value given by two-sided Fisher's exact test.

These data indicate that cohesin controls the connectivity of genes involved in regenerative pathways.

Cohesin-Dependent Long-Range Chromatin Loops Connect Regenerative Gene Promoters with Injury-Responsive Enhancers.

To examine promoter-enhancer loops formed in response to injury, we performed CUT&Tag for H3K27ac from NeuN⁺ sorted neuronal nuclei WT DRG neurons 3 d following SNC versus

homeostasis (sham) (Dataset S3) to map active enhancers (Fig. 3A). PCA and Spearman correlation showed high reproducibility between replicates and clear separation between conditions (SI Appendix, Fig. S13 A and B). Signal intensity of H3K27ac peaks showed enrichment at the level of transcription start sites (TSS) and a high correlation with gene expression, as expected (SI Appendix, Fig. S13C). Genome-wide, differentially expressed genes presented a change in H3K27ac occupancy after nerve injury at the level of

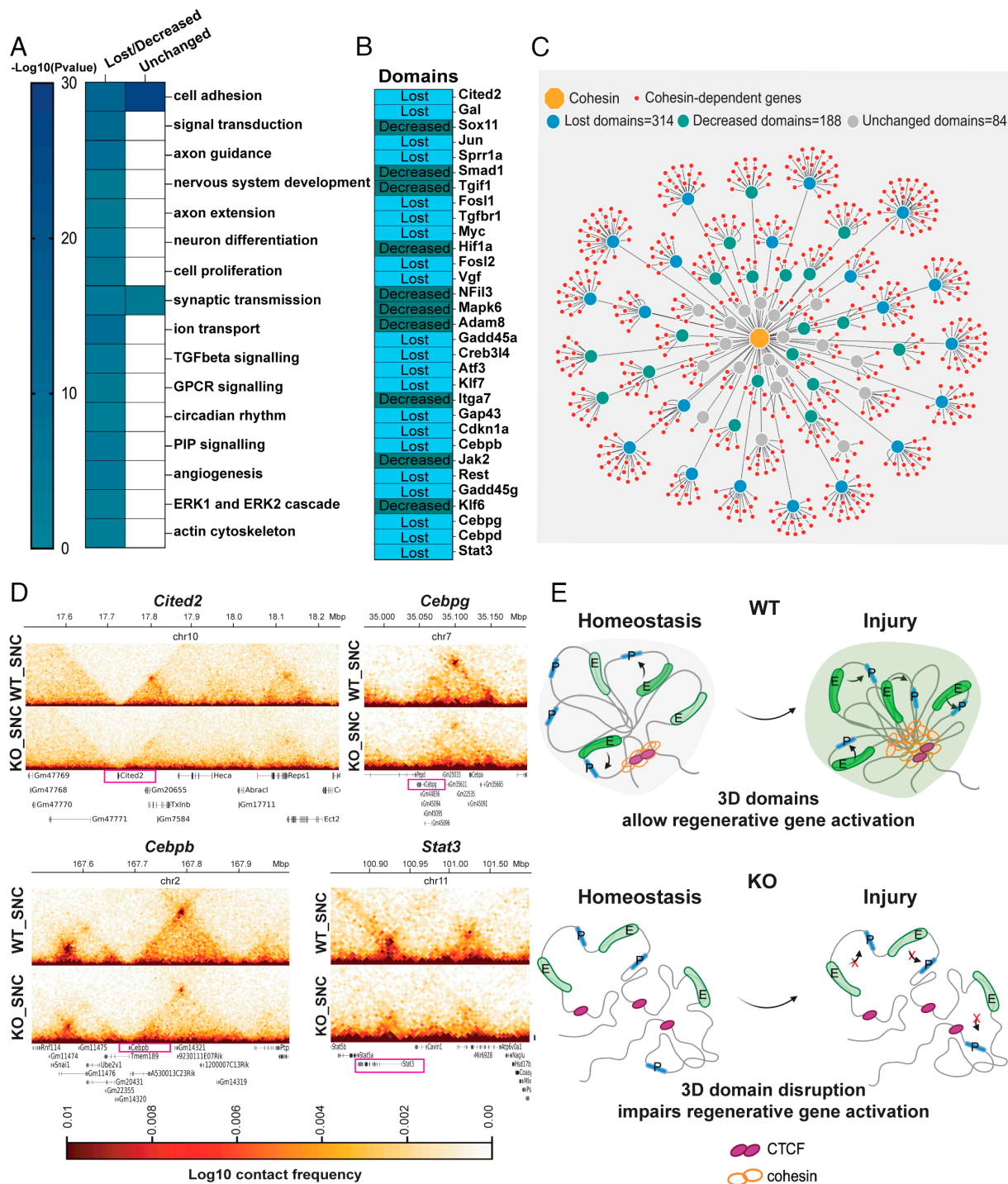


Fig. 4. Regenerative genes reside within cohesin-dependent chromatin domains. (A) Heatmap of the semantically clustered GO biological process categories of the down-regulated genes in *Rad21* KO injured neurons residing within domains that were either lost or showed a decreased contact frequency and unchanged domains. Color code reflects the P -value (modified Fisher's exact $P \leq 0.001$). (B) Heatmap showing the residence of RAGs within genomic domains that were either lost or showed a decreased interaction frequency in *Rad21* KO neurons. (C) Network visualization of the injury-activated, cohesin-dependent genes (red) (cohesin is depicted in orange). Cohesin-dependent genes are preferentially associated with lost domains (blue = 314) and domains with decreased frequency (green = 188) with respect to unchanged domains (gray = 84). Edges connecting the genes to their genomic domains define the fold change of Hi-C interactions in SNC_KO versus SNC_WT. For a better visualization, all the domains on each chromosome are visualized as a unique circle. (D) Example of Hi-C maps of the contact frequency in the indicated conditions within 3D genomic domains. The contacts between the three successive bins (the one containing TSS and its two neighbors) and bins within a genomic distance of 500 Kb are extracted from 5-Kb Hi-C contact matrices. (E) Cohesin facilitates the formation of 3D genomic domains where regenerative genes are coregulated. Loss of cohesin disrupts the architecture of 3D genomic domains impairing the activation of the regenerative program.

TSS and gene bodies (*SI Appendix, Fig. S14A*). Differential H3K27ac occupancy at the TSS correlated well with changes in gene expression (*SI Appendix, Fig. S14 B and C*). Specifically, 454 up-regulated genes correlated with an increased H3K27ac occupancy at the TSS and gene

body regions, and 112 down-regulated with decreased occupancy, respectively (*SI Appendix, Fig. S14D*).

We identified 2,628 H3K27ac peaks displaying increased occupancy and 1,633 decreased occupancy following injury (*SI Appendix,*

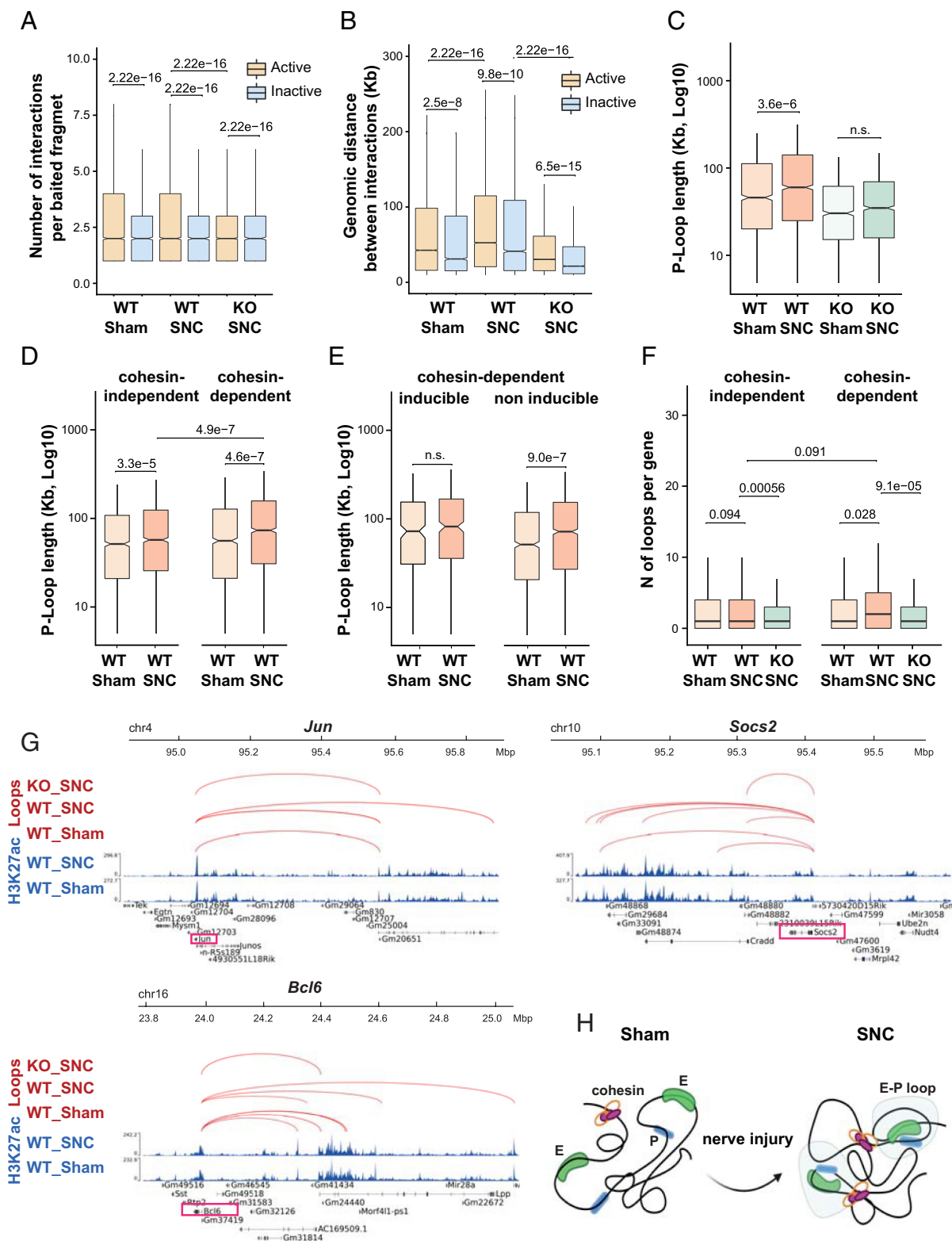


Fig. 5. Cohesin-dependent genes engage in longer chromatin loops in DRG neurons in response to nerve injury. (A and B) Box plot of the number of significant chromatin interactions (A) and the genomic distance between them (B) for inactive (TPM = 0 and first quartile) and active (from second to fourth quartile) genes in the indicated conditions. (C) Box plot of the loop length for up-regulated (FDR < 0.05, FC > 1.5) genes after injury in WT and *Rad21* KO neurons in the indicated conditions. *P*-values are computed from two-sided unpaired Student's *t* test; n.s. = not significant. (D and E) Box plot of the promoter loop length for cohesin-dependent and independent (D) and inducible and noninducible (E) genes in the indicated conditions. *P*-values are computed from two-sided unpaired Student's *t* test; n.s. = not significant. (F) Box plot of the number of promoter loop length per gene for cohesin-dependent and independent genes in the indicated conditions. *P*-values are computed from two-sided unpaired Student's *t* test. (G) Examples of promoter loops at functionally relevant genes. (H) Cohesin facilitates the formation of E-P chromatin loops that allow the activation of the regenerative program after nerve injury.

Fig. S15A, FDR < 0.05). After integrating H3K27ac peaks with data from PCHi-C, we found that chromatin regions in contact with promoters via loops were significantly more associated with H3K27ac peaks with respect to random chromatin regions. These represent neuronal E-P contacts (SI Appendix, Fig. S15B). While most enhancers were involved in more than one interaction (SI Appendix, Fig. S12, Right), WT injured neurons showed a higher number of interactions compared to uninjured control, globally. Indeed, we identified 43,473 and 47,714 E-P loops in WT neurons at homeostasis (sham) and SNC, respectively (Dataset S13). Additionally, more PCHi-C loops associated with increased H3K27ac peaks at the loop anchor were found in WT neurons in SNC compared to Sham, representing loops connecting gene promoters with injury-responsive enhancers (5,794 in SNC, 4,961 in Sham, of which 2,444 in common; Dataset S13). These were associated with increased gene expression (SI Appendix, Fig. S15 C and D).

Similarly to promoter loops, cohesin-dependent, but not cohesin-independent, genes were engaged in longer E-P loops in SNC compared to homeostatic sham condition (SI Appendix, Fig. S15 E and G and Fig. 5G). In particular, genes that were noninducible in response to injury in *Rad21* KO neurons displayed the largest change in loop length after nerve injury in WT neurons with respect to genes that were still partially inducible in *Rad21* KO neurons (SI Appendix, Fig. S15F, 1.02 and 1.35 loop length ratio between SNC versus sham in inducible and noninducible genes, respectively).

Overall, these data indicate that the transcriptional response to nerve injury requires the cohesin-dependent generation of loops connecting regenerative gene promoters to their enhancers for full transcriptional activation (Fig. 5H).

Transcriptional Reprogramming After Injury Is Associated with a More Immature Chromatin Looping Signature. Neuronal regeneration has been associated with a regression toward a transcriptional signature that mimics a less mature developmental state (33, 39). The 3D chromatin architecture changes during neuronal development, with the formation of chromatin loops and domains correlated with neuronal gene activation (42, 44, 45). To explore whether the injury-induced “transcriptional dematuration” involves a change in chromatin looping toward a state resembling a less mature development stage, we leveraged a Hi-C study on nuclei isolated from 18 to 24 wk postconception human fetal cortical plate (the period when neurons are transitioning toward functional maturation) and neurons from the adult prefrontal cortex (45). We found that down-regulated genes after injury preferentially overlapped with genes that were associated with E-P loops that were more specific to adult neurons. Conversely, up-regulated genes after injury, and in particular cohesin-dependent genes, preferentially overlapped with genes that were associated with E-P loops that were more specific to fetal cortical plate (Fig. 6A). Together, these data suggest that injured neurons assume a transcriptional signature associated to a chromatin looping profile similar to that of immature, developing neurons. Down-regulated genes associated with adult human neurons E-P loops were enriched for mature neuron functions, such as ion transport and synaptic transmission; up-regulated genes associated with fetal E-P loops were enriched for genes related to transcription, axon guidance, dendrite morphogenesis, and Ras and VEGF signaling (Fig. 6B).

While in comparison to cohesin-independent genes, cohesin-dependent genes displayed the largest variation in loop length with maturation (Fig. 6C), a reduction in loop length with maturation was also found in constitutive genes, suggesting that this is a developmentally regulated phenomenon (Fig. 6C).

However, constitutive genes did not show any preferential overlap between fetal cortical plate versus adult neurons (Fig. 6A).

These data suggest that the transcriptional dematuration in response to injury is associated with a rewiring of chromatin looping toward a 3D chromatin architecture characteristic of a less mature neuronal developmental stage (Fig. 6D).

Discussion

Our work addressed several outstanding questions. It provided a map of the 3D chromatin architecture of adult mature DRG sensory neurons in vivo at homeostasis and after injury. It showed that the 3D chromatin structure of adult mature neurons responds to injury at the domain and loop level, while A/B compartments remain unaffected. Importantly, chromatin looping rearrangements preferentially occur on regeneration-associated genes and programs and these rearrangements rely on cohesin activity. Additionally, promoter–enhancer loops of adult mature neurons after injury partially recapitulate immature developmental states in the human cortex, where neuronal growth is highest. Last, neuronal conditional cohesin deletion experiments proved that the integrity of 3D chromatin is required for axonal regeneration.

We initially observed that cohesin binding sites are present in a significantly high percentage of neuronal injury-responsive genes. Cohesin generates chromatin loops that facilitate long-range chromatin contacts between gene promoters and their enhancers within 3D genomic domains, and, in collaboration with CTCF, participates in the insulation of such domains (9, 46). Others have shown that coexpression of CTCF with other TFs contributes to promoting axon growth (47). While we also found that injury-responsive genes were enriched for binding sites for CCCTC-binding factor (CTCF), these were significantly less numerous than the ones identified for cohesin. Additionally, while we observed a modest impairment in nerve regeneration after neuronal conditional deletion of CTCF (15), disruption of the cohesin complex via *Rad21* deletion in sensory neurons abrogated nerve regeneration. This prompted us to investigate the role of 3D chromatin folding and cohesin at homeostasis and after nerve injury.

Here, we show that both the integrity of 3D chromatin organization and the formation of long-range chromatin contacts are critical for nerve regeneration. In accordance with previous findings, we observed that cohesin depletion led to loss of 3D genomic domains, without affecting genome compartmentalization (8, 9). Such extensive alteration of 3D genome architecture resulted in the downregulation of genes that support neuronal function, including ion channels, synaptic transmission, and cell adhesion in naïve neurons, similar to what has been found in cortical neurons (41), suggesting that this is a conserved mechanism, supporting its physiological relevance in neuronal homeostasis. However, the most severe changes in gene expression were found after injury, where we observed a further downregulation of neuronal-specific genes and of several transcripts that are normally activated in response to nerve injury in WT neurons. Interestingly, it was recently demonstrated that cohesin is required for gene activation following stimulus rather than constitutive gene expression, for example for the induction of activity-dependent genes in cortical neurons and inflammatory genes in macrophages (41, 48).

Lack of cohesin did not affect all the genes that are activated in response to injury. While genes that are involved in immune and inflammatory functions were independent from cohesin for their activation, genes affected by cohesin depletion were enriched for biological pathways that have been reported to be pro-regenerative (15, 31, 32, 39, 40). These included a high proportion of RAGs (13, 14), which were found enriched within chromatin contacts

mechanisms in the regenerative failure of central axons, and whether these mechanisms can be harnessed to enhance sensory recovery after peripheral or central lesions.

Methods

Method Summary. WT and *Rad21* KO mice underwent SNC injury or sham. In regeneration experiments, axon regeneration was assessed at 7 and 18 d postinjury. In epigenomics experiments, 3 d postinjury DRG neuronal nuclei were assessed via combinatorial Hi-C, promoter-capture Hi-C, CUT&Tag for H3K27ac and RNA-seq. Detailed descriptions of experimental methodologies used in the study are provided in *SI Appendix, Supplementary Methods*.

Replication. All attempts of replication were successful.

Blinding. All assessments were performed in blind by two independent experimenters.

Data, Materials, and Software Availability. Data have been deposited at the Gene Expression Omnibus (GEO) under accession ID [GSE249687](https://www.ncbi.nlm.nih.gov/geo/query/acc.cgi?acc=GSE249687) (53). All the accession codes used for this study are [GSE84176](https://www.ncbi.nlm.nih.gov/geo/query/acc.cgi?acc=GSE84176) (54), [GSE59119](https://www.ncbi.nlm.nih.gov/geo/query/acc.cgi?acc=GSE59119) (55), [GSE96107](https://www.ncbi.nlm.nih.gov/geo/query/acc.cgi?acc=GSE96107) (56), [GSE126957](https://www.ncbi.nlm.nih.gov/geo/query/acc.cgi?acc=GSE126957) (57), [GSE142881](https://www.ncbi.nlm.nih.gov/geo/query/acc.cgi?acc=GSE142881) (58), and [syn4921369](https://www.ncbi.nlm.nih.gov/geo/query/acc.cgi?acc=syn4921369) (59). RNA sequencing; Hi-C, promoter-capture Hi-C, CUT&Tag for H3K27ac; and computer programs for processing and analysing the data have been deposited in GEO ([GSE249687](https://www.ncbi.nlm.nih.gov/geo/query/acc.cgi?acc=GSE249687)) (53); GitHub

(<https://github.com/zwang-bioinformatics/RAD21-2024/>) (60). All other data are included in the manuscript and/or [supporting information](#).

ACKNOWLEDGMENTS. We thank the LMS/NIHR Imperial Biomedical Research Centre Flow Cytometry Facility for nuclear sorting. We thank Dr. Maria Teresa Cencioni at Imperial College London with assistance in flow cytometry analysis of sorted nuclear fractions. This work was supported by The Rosetrees Trust (S.D.G.), the MRC (S.D.G.), Wings For Life (S.D.G.), the NIH Research (NIHR) Imperial Biomedical Research Centre (S.D.G.), the National Institute of General Medical Sciences Grant (1R35GM137974 to Z.W.), and Ohio State University start-up (PG100125 to I.P.). The views expressed are those of the author(s) and not necessarily those of the NHS, the NIHR, or the Department of Health.

Author affiliations: ^aDepartment of Medicine, Division of Brain Sciences, Centre for Restorative Neuroscience, Imperial College London, London W12 0NN, United Kingdom; ^bDepartment of Neuroscience, Department of Plastic and Reconstructive Surgery, The Ohio State University, Columbus, OH 43210; ^cDepartment of Computer Science, University of Miami, Coral Gables, FL 33124-4245; and ^dThe Institute of Clinical Sciences, Medical Research Council, Laboratory of Medical Sciences, Faculty of Medicine, Imperial College London, London W12 0NN, United Kingdom

Author contributions: I.P. conceived the idea; I.P., T.L., Z.W., and S.D.G. designed research; I.P., W.G., L.Z., F.M., J.C., R.T.R., G.K., Y.Y., S.G., and F.D.V. performed research; I.P., T.L., W.G., M.M., R.T.R., J.W.D.K., E.A.-j., A.C., B.C., and E.D.V. analyzed data; I.P., Z.W., and S.D.G. provided funding; and I.P., T.L., and S.D.G. wrote the paper.

1. A. S. Hansen, C. Cattoglio, X. Darzacq, R. Tjian, Recent evidence that TADs and chromatin loops are dynamic structures. *Nucleus* **9**, 20–32 (2018).
2. J. R. Dixon *et al.*, Topological domains in mammalian genomes identified by analysis of chromatin interactions. *Nature* **485**, 376–380 (2012).
3. E. P. Nora *et al.*, Spatial partitioning of the regulatory landscape of the X-inactivation centre. *Nature* **485**, 381–385 (2012).
4. S. S. Rao *et al.*, A 3D map of the human genome at kilobase resolution reveals principles of chromatin looping. *Cell* **159**, 1665–1680 (2014).
5. R. A. Beagrie, A. Pombo, Gene activation by metazoan enhancers: Diverse mechanisms stimulate distinct steps of transcription. *BioEssays: News and reviews in molecular. Cell. Dev. Biol.* **38**, 881–893 (2016).
6. A. Panigrahi, B. W. O'Malley, Mechanisms of enhancer action: The known and the unknown. *Genome Biol.* **22**, 108 (2021).
7. E. P. Nora *et al.*, Targeted degradation of CTCF decouples local insulation of chromosome domains from genomic compartmentalization. *Cell* **169**, 930–944.e922 (2017).
8. W. Schwarzer *et al.*, Two independent modes of chromatin organization revealed by cohesin removal. *Nature* **551**, 51–56 (2017).
9. S. S. P. Rao *et al.*, Cohesin loss eliminates all loop domains. *Cell* **171**, 305–320.e324 (2017).
10. J. Zuin *et al.*, Cohesin and CTCF differentially affect chromatin architecture and gene expression in human cells. *Proc. Natl. Acad. Sci. U.S.A.* **111**, 996–1001 (2014).
11. A. L. Sanborn *et al.*, Chromatin extrusion explains key features of loop and domain formation in wild-type and engineered genomes. *Proc. Natl. Acad. Sci. U.S.A.* **112**, E6456–E6465 (2015).
12. G. Fudenberg *et al.*, Formation of chromosomal domains by loop extrusion. *Cell Rep.* **15**, 2038–2049 (2016).
13. V. Chandran *et al.*, A systems-level analysis of the peripheral nerve intrinsic axonal growth program. *Neuron* **89**, 956–970 (2016).
14. T. C. Ma, D. E. Willis, What makes a RAG regeneration associated? *Front. Mol. Neurosci.* **8**, 43 (2015).
15. I. Palmisano *et al.*, Epigenomic signatures underpin the axonal regenerative ability of dorsal root ganglia sensory neurons. *Nat. Neurosci.* **22**, 1913–1924 (2019).
16. Y. L. Weng *et al.*, An intrinsic epigenetic barrier for functional axon regeneration. *Neuron* **94**, 337–346.e336 (2017).
17. M. J. Finelli, J. K. Wong, H. Zou, Epigenetic regulation of sensory axon regeneration after spinal cord injury. *J. Neurosci.* **33**, 19664–19676 (2013).
18. P. Gaub *et al.*, HDAC inhibition promotes neuronal outgrowth and counteracts growth cone collapse through CBP/p300 and P/CAF-dependent p53 acetylation. *Cell Death Differ.* **17**, 1392–1408 (2010).
19. R. Puttagunta *et al.*, P/CAF-dependent epigenetic changes promote axonal regeneration in the central nervous system. *Nat. Commun.* **5**, 3527 (2014).
20. P. Gaub *et al.*, The histone acetyltransferase p300 promotes intrinsic axonal regeneration. *Brain* **134**, 2134–2148 (2011).
21. Y. Cho, R. Sloutsky, K. M. Naegle, V. Cavalli, Injury-induced HDAC5 nuclear export is essential for axon regeneration. *Cell* **155**, 894–908 (2013).
22. A. Hervera *et al.*, PP4-dependent HDAC3 dephosphorylation discriminates between axonal regeneration and regenerative failure. *EMBO J.* **38**, e101032 (2019), [10.15252/embj.2018101032](https://doi.org/10.15252/embj.2018101032).
23. Y. M. Oh *et al.*, Epigenetic regulator UHRF1 inactivates REST and growth suppressor gene expression via DNA methylation to promote axon regeneration. *Proc. Natl. Acad. Sci. U.S.A.* **115**, E12417–E12426 (2018).
24. I. Palmisano, S. Di Giovanni, Advances and limitations of current epigenetic studies investigating mammalian axonal regeneration. *Neurotherapeutics* **15**, 529–540 (2018).
25. Y. E. Loh *et al.*, Comprehensive mapping of 5-hydroxymethylcytosine epigenetic dynamics in axon regeneration. *Epigenetics* **12**, 77–92 (2017).
26. R. Lindner, R. Puttagunta, T. Nguyen, S. Di Giovanni, DNA methylation temporal profiling following peripheral versus central nervous system axotomy. *Sci. Data* **1**, 140038 (2014).
27. E. E. Ewan *et al.*, Ascending dorsal column sensory neurons respond to spinal cord injury and downregulate genes related to lipid metabolism. *Sci. Rep.* **11**, 374 (2021).
28. D. S. Sams *et al.*, Neuronal CTCF is necessary for basal and experience-dependent gene regulation, memory formation, and genomic structure of BDNF and Arc. *Cell Rep.* **17**, 2418–2430 (2016).
29. J. D. Ziebarth, A. Bhattacharya, Y. Cui, CTCFBSDB 2.0: A database for CTCF-binding sites and genome organization. *Nucleic Acids Res.* **41**, D188–D194 (2013).
30. A. Cuadrado, S. Remeseiro, O. Grana, D. G. Pisano, A. Losada, The contribution of cohesin-SA1 to gene expression and chromatin architecture in two murine tissues. *Nucleic Acids Res.* **43**, 3056–3067 (2015).
31. A. Hervera *et al.*, Reactive oxygen species regulate axonal regeneration through the release of exosomal NADPH oxidase 2 complexes into injured axons. *Nat. Cell Biol.* **20**, 307–319 (2018).
32. F. De Virgiliis *et al.*, The circadian clock time tunes axonal regeneration. *Cell Metab.* **35**, 2153–2164.e2154 (2023).
33. G. H. D. Poplawski *et al.*, Injured adult neurons regress to an embryonic transcriptional growth state. *Nature* **581**, 77–82 (2020).
34. Y. Cheng *et al.*, Transcription factor network analysis identifies REST/NRSF as an intrinsic regulator of CNS regeneration in mice. *Nat. Commun.* **13**, 4418 (2022).
35. V. C. Seitan *et al.*, A role for cohesin in T-cell-receptor rearrangement and thymocyte differentiation. *Nature* **476**, 467–471 (2011).
36. J. E. Shin, S. Geisler, A. DiAntonio, Dynamic regulation of SCG10 in regenerating axons after injury. *Exp. Neurol.* **252**, 1–11 (2014).
37. A. Mo *et al.*, Epigenomic signatures of neuronal diversity in the mammalian brain. *Neuron* **86**, 1369–1384 (2015).
38. J. Lau *et al.*, Temporal control of gene deletion in sensory ganglia using a tamoxifen-inducible Advillin-Cre-ERT2 recombinase mouse. *Mol. Pain* **7**, 100 (2011).
39. A. Tedeschi *et al.*, The calcium channel subunit Alpha2delta2 suppresses axon regeneration in the adult CNS. *Neuron* **92**, 419–434 (2016).
40. W. Renthall *et al.*, Transcriptional reprogramming of distinct peripheral sensory neuron subtypes after axonal injury. *Neuron* **108**, 128–144.e129 (2020).
41. L. Calderon *et al.*, Cohesin-dependence of neuronal gene expression relates to chromatin loop length. *eLife* **11**, e76539 (2022).
42. B. Bonev *et al.*, Multiscale 3D genome rewiring during mouse neural development. *Cell* **171**, 557–572.e524 (2017).
43. J. Cairns *et al.*, CHICAGO: Robust detection of DNA looping interactions in Capture Hi-C data. *Genome Biol.* **17**, 127 (2016).
44. X. Luo *et al.*, 3D genome of macaque fetal brain reveals evolutionary innovations during primate corticogenesis. *Cell* **184**, 723–740.e721 (2021).
45. S. Rahman *et al.*, Lineage specific 3D genome structure in the adult human brain and neurodevelopmental changes in the chromatin interactome. *Nucleic Acids Res.* **51**, 11142–11161 (2023), [10.1093/nar/gkad798](https://doi.org/10.1093/nar/gkad798).
46. M. Merkschlagger, E. P. Nora, CTCF and cohesin in genome folding and transcriptional gene regulation. *Annu. Rev. Genom. Hum. Genet.* **17**, 17–43 (2016).
47. O. Avraham *et al.*, Analysis of neuronal injury transcriptional response identifies CTCF and YY1 as co-operating factors regulating axon regeneration. *Front. Mol. Neurosci.* **15**, 967472 (2022).
48. S. Cuartero *et al.*, Control of inducible gene expression links cohesin to hematopoietic progenitor self-renewal and differentiation. *Nat. Immunol.* **19**, 932–941 (2018).
49. I. Venkatesh, V. Mehra, Z. Wang, B. Califf, M. G. Blackmore, Developmental chromatin restriction of pro-growth gene networks acts as an epigenetic barrier to axon regeneration in cortical neurons. *Dev. Neurobiol.* **78**, 960–977 (2018).
50. Y. Fujita *et al.*, Decreased cohesin in the brain leads to defective synapse development and anxiety-related behavior. *J. Exp. Med.* **214**, 1431–1452 (2017).
51. B. Hu *et al.*, Neuronal and glial 3D chromatin architecture informs the cellular etiology of brain disorders. *Nat. Commun.* **12**, 3968 (2021).
52. F. D. Weiss *et al.*, Neuronal genes deregulated in Cornelia de Lange Syndrome respond to removal and re-expression of cohesin. *Nat. Commun.* **12**, 2919 (2021).

53. I. Palmisano, T. Liu, S. Di Giovanni, Z. Wang, Three-dimensional chromatin architecture in DRG neurons following sciatic nerve injury in WT and Rad21 KO mice. *Gene Expression Omnibus*. <https://www.ncbi.nlm.nih.gov/geo/query/acc.cgi?acc=GSE249687>. Deposited 8 December 2023.
54. D. S. Sams *et al.*, CTCF ChIP-seq of WT and RNA-seq of WT and CTCF cko mouse. *Gene Expression Omnibus*. <https://www.ncbi.nlm.nih.gov/geo/query/acc.cgi?acc=GSE84176>. Deposited 8 July 2016.
55. A. Cuadrado, A. Losada, S. Remeseiro, O. Graña, D. G. Pisano, The contribution of cohesin-SA1 to chromatin architecture and gene expression in two murine tissues. *Gene Expression Omnibus*. <https://www.ncbi.nlm.nih.gov/geo/query/acc.cgi?acc=GSE59119>. Deposited 7 July 2014.
56. B. Bonev *et al.*, Multi-scale 3D genome rewiring during mouse neural development. *Gene Expression Omnibus*. <https://www.ncbi.nlm.nih.gov/geo/query/acc.cgi?acc=GSE96107>. Deposited 11 March 2017.
57. G. H. Poplawski, R. Kawaguchi, G. Coppola, M. Tuszynski, The regeneration transcriptome of corticospinal neurons. *Gene Expression Omnibus*. <https://www.ncbi.nlm.nih.gov/geo/query/acc.cgi?acc=GSE126957>. Deposited 22 February 2019.
58. Y. Cheng *et al.*, Transcriptional profiling of adult retinal ganglion cells during optic nerve regeneration. *Gene Expression Omnibus*. <https://www.ncbi.nlm.nih.gov/geo/query/acc.cgi?acc=GSE142881>. Deposited 2 January 2020.
59. S. Rahman *et al.*, Lineage specific 3D genome structure in the adult human brain and neurodevelopmental changes in the chromatin interactome. *PsychENCODE Knowledge Portal*. <https://www.synapse.org/Synapse:syn26164834>. Deposited 5 October 2021.
60. L. Tong, Z. Wang, RAD21-2024. *GitHub*. <https://github.com/zwang-bioinformatics/RAD21-2024/>. Deposited 12 June 2024.